HHS Public Access

Author manuscript

J Neurosci Res. Author manuscript; available in PMC 2019 September 01.

Published in final edited form as:

J Neurosci Res. 2019 March ; 97(3): 313–331. doi:10.1002/jnr.24352.

Ablation of Cytoskeletal Scaffolding Proteins, Band 4.1B and Whirlin, Leads to Cerebellar Purkinje Axon Pathology and Motor Dysfunction

Julia Saifetiarova and **Manzoor A. Bhat**

Department of Cellular and Integrative Physiology, Center for Biomedical Neuroscience, Long School of Medicine, University of Texas Health Center, 7703 Floyd Curl Drive, San Antonio, TX 78229-3900, USA

Abstract

The cerebellar cortex receives neural information from other brain regions to allow fine motor coordination and motor learning. The primary output neurons from the cerebellum are the Purkinje neurons that transmit inhibitory responses to deep cerebellar nuclei through their myelinated axons. Altered morphological organization and electrical properties of the Purkinje axons lead to detrimental changes in locomotor activity often leading to cerebellar ataxias. Two cytoskeletal scaffolding proteins Band 4.1B (4.1B) and Whirlin (Whrn) have been previously shown to play independent roles in axonal domain organization and maintenance in myelinated axons in the spinal cord and sciatic nerves. Immunoblot analysis had indicated cerebellar expression for both 4.1B and Whrn, however, their subcellular localization and cerebellum specific functions have not been characterized. Using *4.1B* and *Whrn* single and double mutant animals, we show that both proteins are expressed in common cellular compartments of the cerebellum and play cooperative roles in preservation of the integrity of Purkinje neuron myelinated axons. We demonstrate that both 4.1B and Whrn are required for the maintenance of axonal ultrastructure and health. Loss of 4.1B and Whrn leads to axonal transport defects manifested by formation of swellings containing cytoskeletal components, membranous organelles and vesicles. Moreover, ablation of both proteins progressively affects cerebellar function with impairment in locomotor performance

[#]**Address correspondence to:** Manzoor A. Bhat, M.S., Ph.D., University of Texas Health Science Center, 7703 Floyd Curl Drive, San Antonio, TX 78229-3900, USA, Tel: 1-210-567-4325, Fax: 1-210-567-4410, bhatm@uthscsa.edu.

Author Contributions

All authors in this study take responsibility for integrity of the research, as well as for accuracy of data acquisition and analysis.

Conceptualization, J.S. and M.A.B.;
Methodology, J.S. and M.A.B.;
Investigation, J.S.;
Formal Analysis, J.S.;
Resources, M.A.B.;
Writing – Original Draft, J.S. and M.A.B.;
Writing – Review & Editing, J.S. and M.A.B.;
Visualization, J.S.;
Supervision and Funding acquisition, M.A.B.

Associate Editor: Dr. Scott Brady

Conflict of Interest

The authors declare no competing financial interests.

Data Accessibility

Following tools and software were used in the current study: ImageJ, RRID:SCR_003070 for images analysis (https://imagei.nih.gov/ij/); Graphpad Prism, RRID:SCR_002798 for statistical analysis (http://graphpad.com/).

detected by altered gait parameters. Together, our data indicate that 4.1B and Whrn are required for maintaining proper axonal cytoskeletal organization and axonal domains, which is necessary for cerebellum controlled fine motor coordination.

Graphical Abstract

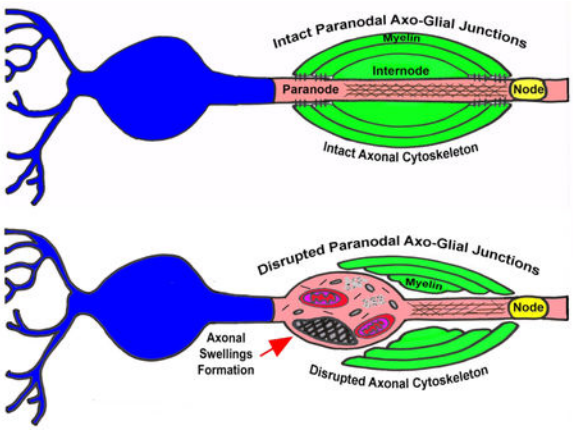

Purkinje neurons myelinated fibers require intact axonal cytoskeletal organization and axonal transport to effectively transmit neural signals. We show that proteins Band 4.1B and Whirlin cooperatively maintain axonal cytoskeletal integrity at the paranodal and juxtaparanodal regions, and their loss leads to axonal cytoskeletal disorganization and formation of swellings leading to axonal degeneration.

Keywords

Cerebellum; Motor Coordination; Purkinje Neurons; Myelinated Axons; Axonal Degeneration; Band 4.1B; Whirlin

INTRODUCTION

Neuronal signals are transmitted in a fast and efficient manner in the form of action potentials along myelinated axons, which are uniquely organized into distinct molecular domains: the nodes of Ranvier, paranodes, juxtaparanodes and internodes. Proper organization of the axonal cytoskeleton along the axon and specifically at these domains underlies the integrity of each molecular domain, provides structural support and is required to maintain axonal transport, which is vital for neuronal functions (Kevenaar and Hoogenraad, 2015). Disorganization of the axonal cytoskeletal structure causes disintegration of the axonal domains, which in turn negatively affects conductive properties of the myelinated fibers. Additionally, disrupted cytoskeletal organization affects axonal transport leading to accumulation of swellings filled with protein aggregates and membranous organelles, which results in loss of trophic support of neuronal fibers and terminals (Millecamps and Julien, 2013; Perlson et al., 2010). Thus, impaired cytoskeletal structure of the axon has been linked as a common factor in such neurodegenerative disorders as Charcot-Marie-Tooth peripheral neuropathy (Brownlees et al., 2002; Misko et

al., 2010), Parkinson's (Abou-Sleiman et al., 2006; Saha et al., 2004) and Huntington's disease (McGuire et al., 2006; Morfini et al., 2009), Alzheimer's disease and other dementias (Kamal et al., 2001; Morfini et al., 2007).

Two cytoskeletal scaffolding proteins Band 4.1B (4.1B) and Whirlin (Whrn), have been shown to preserve the stereotypic organization of myelinated fibers. 4.1B is localized to paranodes, juxtaparanodes and internodes, and links various transmembrane proteins, such as Contactin-associated protein 1 (Caspr1), Caspr2, and Nectin-like proteins to actin/spectrin cytoskeleton through their FERM-binding domains (Buttermore et al., 2011; Cifuentes-Diaz et al., 2011; Denisenko-Nehrbass et al., 2003; Einheber et al., 2013; Horresh et al., 2010; Sun et al., 2002). Loss of 4.1B leads to disorganization of juxtaparanodal region and loss of paranodal axo-glial septate junctions in both PNS and CNS (Buttermore et al., 2011). On the other hand, the functions of Whrn scaffold in axonal domain maintenance as a cytoskeletal linker have revealed its role in paranodal compaction and stabilization of the axonal cytoskeleton (Green et al., 2013). Previously, it was reported that Whrn plays an important role in visual and auditory system (Mburu et al., 2006; Yang et al., 2010). Mutations in humans *WHRN* have been linked to Usher syndrome Type II, which is an autosomal recessive vision-hearing impairment disorder (Friedman et al., 2011; van Wijk et al., 2006). In addition, it has been previously reported that in the auditory system, Whrn and 4.1B indirectly interact with each other through the membrane-associated guanylate kinase protein p55 and that loss of Whrn leads to complete ablation of 4.1B expression at the apical surface of cochlear hair cells (Okumura et al., 2010). Since other binding partners of Whrn complex in the PNS and CNS are yet to be completely elucidated, we wanted to determine whether 4.1B and Whrn function together to maintain the cytoskeletal organization of myelinated axons.

Using *4.1B* and *Whrn* single and double mutants, we report that single or combined loss of cytoskeletal scaffolding proteins 4.1B and Whrn leads to destabilization of axonal domains in the cerebellar white matter, consequently altering ultrastructural organization of axonal domains in myelinated fibers. Loss of these proteins also disrupts axonal transport in the Purkinje cells and causes formation of axonal swellings, accumulation of membranous organelles, transport vesicles and neurofilament aggregates along the axons. These data highlight the essential role of these cytoskeletal scaffolding proteins in the proper organization and maintenance of normal axonal structure in myelinated nerve fibers.

MATERIALS AND METHODS

Animals

To obtain *4.1B* null mutants *(4.1B KO), 4.1B*^{Flox} mice described previously (Buttermore et al., 2011) were crossed to *Actin-Cre* animals (RRID:IMSR_JAX:019099) to ubiquitously recombine one of the *Flox* alleles. *Actin-Cre,4.1B*^{Flox} mice were crossed to wild type mice in a mixed *C57BL/6* and *129/Sv* genetic background to generate *4.1B KO* mice. *Whrn* exon 1 homozygous deletion mutants *(WKO)* were obtained from Dr. Jun Yang's laboratory and were described previously (Green et al., 2013; Yang et al., 2010). *4.1B/WKO* heterozygous mice were mated to obtain *4.1B/WKO* double knockout animals (*dKO*). PCR primers used for genotyping were as follows: *4.1B* FP: `5′ -TAG GCA TGT CAGGAGAGCCAT GCAT-3′`

or 5′-TTT ACG GTA TCG CCG CTC CCG ATT-3′ with a common *4.1B* RP: 5′- TGT ATG GCT GAA TCCCAT GCA GGG-3′ to amplify 246 bp wild type or 550 bp null mutant band, respectively. For *Whrn* FP: 5′-GGG TGA GTG AAT GCC AGC CAC-3′ or 5′-GAG ATC AGC AGC CTC TGT TCC AC-3′ together with RP 5′-CAG GGA AGT TGA GGC ACA CGG-3′ were used to amplify an 894 bp wild type and 700 bp mutant bands, respectively.

Mice were maintained under controlled temperature conditions (21–23 °C) and 12 hour light cycle (lights on 8 am – 8 pm) with ad libitum access to food and water. To track the progression of phenotypes, equal number of males and females were analyzed at two and six months of age in each group. Prior to tissue collection animals were anesthetized with i.p. Avertin injection (400mg/kg body weight). All animal experiments were performed according to NIH and Institutional Animal Care and Use Committee approved guidelines for ethical treatment of laboratory animals at the University of Texas Health Science Center at San Antonio. For phenotypic characterization, no animals were excluded from statistical data analysis.

Antibodies

Guinea pig anti-Caspr1 (Bhat et al., 2001), guinea pig anti-4.1B(Buttermore et al., 2011), guinea pig anti-Whrn (Green et al., 2013), rabbit anti-βIV Spectrin (βIV Spec) (Saifetiarova et al., 2017b), rat anti-pan Neurofascin (NFCt, recognizing the c-terminus) (Taylor et al., 2017) antibodies have been described previously. Other primary antibodies used for experiments are: a) mouse anti-potassium voltage-gated channel subfamily A member 2 (K_V1.2) (UC Davis/NIH NeuroMab Facility Cat# 75-008 RRID:AB_2296313); b) mouse anti-Neurofilament (Covance Research Products Inc Cat# SMI-312R RRID:AB_2315329); c) mouse anti-Calbindin (Calb) Sigma-Aldrich Cat# C9848, RRID:AB_476894); d) rabbit anti-Calb antibodies (Millipore Cat# AB1778, RRID:AB_2068336); e) mouse anti-β-Actin antibodies (Sigma-Aldrich Cat# A5441, RRID:AB_476744); f) rabbit anti-Caspr2 antibodies (Abeam Cat# ab33994, RRID:AB_2083506); and g) secondary antibodies for immunostaining (Alexa Fluor- 488, 568, 647) were purchased from Invitrogen (USA); e) IR-conjugated secondary antibodies for immunoblotting were purchased from LI-COR (USA).

Tissue Preparation and Immunostaining

Animals were anesthetized with i.p. injection of Avertin (400mg/kg body weight) of and transcardially perfused with phosphate-buffered saline (PBS) (pH 7.2-7.4) followed by ice-cold 4% paraformaldehyde in PBS solution (pH 7.2-7.4). Cerebellums (CB) were dissected out and postfixed in the same fixative for 12 hours at 4°C. Further, CB tissue was rinsed several times and 50μm sections were cut with a Vibratome and kept in PBS at 4°C until further processing for immunostaining.

Immunoblotting

Samples were processed as described previously (Saifetiarova et al., 2017b). Briefly, mouse cerebellums were dissected out and homogenized on ice in lysis buffer. Homogenized samples were incubated at 4°C followed by centrifugation at 20,000g at 4°C for 30 minutes. Supernatant was collected as a final lysate, boiled for 5 min at 100°C, loaded on SDS-PAGE, transferred to nitrocellulose and probed with primary antibodies. Afterwards membranes

were incubated in IR-conjugated secondary antibodies followed by detection using Odyssey® CLx Imaging System. Band intensities standardized to α-Tubulin were quantified and averaged from 3 independent experiments.

Transmission Electron Microscopy

Transmission electron microscopy (TEM) of CBs from *wt, 4.1B KO, WKO* and *dKO* mice was performed as described previously (Saifetiarova et al., 2017b; Taylor et al., 2017). Briefly, the animals (3 mice/genotype) were anesthetized with i.p. Avertin injection (400mg/kg body weight) and transcardially perfused with freshly prepared normal saline followed by 2.5%glutaraldehyde/4%PFA dissolved in 0.16 M NaH_2PO_4/0.11M NaOH buffer (final pH 7.2-7.4) EM fixative for 30 minutes. After perfusion, mouse carcasses were post-fixed for another 2 weeks in the same EM fixative. Afterwards, CBs were dissected out and incubated overnight in 0.1M sodium cacodylate buffer followed by incubation in 2% OsO_4 solution and gradient ethanol dehydration. Samples were incubated in propylene oxide, left in 100% PolyBed resin with constant agitation for 36 hours and embedded in flat molds at 55°C for 36 hours. After embedding, the molds were processed and imaged on a JEOL 1230 electron microscope at the UTHSCSA Electron Microscopy Lab.

Analysis of Paranodal and Juxtaparanodal Phenotypes in Myelinated Axons

For evaluation of percentage of abnormal paranodal and juxtaparanodal phenotypes, cerebellar slices were immunostained with Caspr1 and Kv1.2 antibodies. Images were acquired by Zeiss LSM 710 confocal microscope with 40x magnification objective using identical settings. On average, 3 confocal images from cerebellar lobule VIa white matter were randomly taken and localization of Caspr1 and Kv1.2 channels was analyzed per field of view. In detail assessed phenotypes are described in Fig. 2I. Final data is represented as a scatter plot with individual values averaged from 3 confocal images per animal, where % of abnormal para- or juxtaparanodes for each animal is = [number of abnormal para- or juxtaparanodes/field of view]/ [total number of para- or juxtaparanodes/field of view] × 100%.

Analysis of Size and Density of Swellings along the Purkinje Axons in the Cerebellum

For quantification of size and density of the swellings, each subsequent 50 μm-thick cerebellar slice was collected and immunostained with Calbindin antibodies. Three slices/ animal were collected and 1 confocal image of cerebellar lobule Via/slice was acquired by Zeiss LSM 710 confocal microscope with 10X magnification. Calbindin positive bead-like axonal swellings were selected and their area was manually measured using freeform drawing tool in ImageJ software. Averaged area of the swellings from each animal was plotted. Density of swellings from the lobule Via was quantified from the same set of images by using following formula: density of swellings = total number of swellings/ lobule VIa area.

Catwalk Gait Analysis

The Catwalk automated gait analysis system (Noldus, Wageningen, Netherlands) was used to assess the gait and motor coordination in *wild type (wt), 4.1B KO, WKO* and *dKO*

animals at two and six months of age. The apparatus consists of a glass plate walkway with a fluorescent light beaming into the glass from the side. As the mouse crosses the walkway fluorescent light illuminates the animal's paws and when the paw touches the glass a bright print image of it is being produced (Hamers et al., 2001). Catwalk XT 10.6 software (Noldus, Wageningen, The Netherlands) was used to record and process the position of footprints allowing quantitative analysis of gait. All mice were trained to cross the walkway for at least three times a day over four successive days. On the final day of acquisition, data were collected from three replicate crossings by each mouse on day 5. A successful run was defined as animal crosses the runway without any interruption. The following parameters were quantified: run average speed (cm/s), base of support for front and hind paws (cm), mean of the footprint's maximal intensity for each paw, stride length (cm).

Statistics

Data measurements and analysis were performed by one examiner in a non-blinded manner. All data are presented as scatter plots with mean ± SD and n represents the number of animals (unless otherwise stated). Three animals per group (with at least 300 quantified paranodes and juxtaparanodes per animal) were analyzed for paranodal/juxtaparanodal phenotype and immunoblot analysis, and 5-7 animals for catwalk measurements. Unless shown otherwise, statistically significant differences between mutant and control groups were determined by 2-way ANOVA (age and genotype as two independent variables) with Bonferroni's post hoc test using GraphPad Prism5 software and are represented by *P<0.05; **P<0.01; ***P<0.001.

Results

Band 4.1B and Whirlin Expression and Subcellular Localization in the Cerebellum

4.1B and Whrn, as cytoskeletal proteins have been previously shown to be abundantly expressed in the mouse cerebellum by Western Blot analysis or mRNA *in situ* hybridization (Parra et al., 2000; Wang et al., 2012), however, their detailed cerebellar sub-cellular localization has not been evaluated. To determine their expression and localization in the cerebellum, we immunostained two-month-old (mo) cerebellar slices from the *wt, 4.1B* and *Whrn* single and double mutants using 4.1B or Whrn antibodies in combination with other markers. Immunostaining of sagittal cerebellar slices with Whrn and Calbindin antibodies revealed that it is abundantly expressed throughout molecular, Purkinje cell and granule cell layers in control mice (Fig. 1A). Specifically, its expression was enriched in the Bergmann glia soma and processes, Purkinje cells soma and dendrites as well as in the granule cell soma and their axons, forming parallel fibers in the molecular layer of the cerebellum (Fig. 1A). Identical immunostaining of *4.1B KO* mice cerebellums revealed reduction in the areas, which were enriched with Whrn in control slices (Fig. 1B). As expected, in single *WKO* and *dKO* mice, Whrn immunoreactivity was not detected, except residual background staining (Fig. 1C, D). Next, we performed immunostaining of cerebellar slices with combination of antibodies against 4.1B and Calbindin. As shown in Fig. 1E in *wt* animals, 4.1B was heavily expressed in molecular layer (parallel fibers and soma of the interneurons), in the Purkinje cell soma and dendrites, as well as in the granule cells soma and mossy fibers synapses. Analysis of 4.1B expression in other genotypes revealed, as expected its absence in the

single *4.1B KO* and *dKO* animals (Fig. 1F, H), and reduced expression pattern in the *WKO* mice (Fig. 1G). It has been shown previously that 4.1B localization in the inner ear hair cells is Whrn dependent (Okumura et al., 2010), and these two proteins may indirectly interact and form a complex through the membrane-associated guanylate kinase protein p55. However, we did not find co-localization of p55 with 4.1B or Whrn in the cerebellum of any studied genotypes (*data not shown*). Further, we investigated localization of 4.1B and Whrn in the cerebellar white matter tracts. In *wt* and *4.1B KO* tissue, Whrn immunostaining showed that it is evenly distributed along myelinated axons and co-localizes with Caspr1 at the paranodes and also with Calbindin along the axon (Fig. 1I, J), and as expected it was absent in *WKO* and *dKO* mice (Fig. 1K, L). Similarly, immunostaining of the cerebellar myelinated fibers against 4.1B in the *wt* and *WKO* mice showed its distribution along the axons, except nodal areas (Fig. 1M, O). Moreover, a slight increase in 4.1B fluorescence intensity was observed in the *WKO* myelinated axons, which might be caused by either mislocalization or accumulation of 4.1B in the absence of Whrn (Fig. 1O). As expected, 4.1B immunoreactivity was absent in *4.1B* single or *dKO* myelinated axons (Fig. 1N, P). Together, the immunolocalization data show that both 4.1B and Whrn are abundantly expressed in all cerebellar layers and that they display an interdependent subcellular localization.

Paranodal and Juxtaparanodal Domains are Severely Affected in the Absence of Band 4.1B and Whrn

4.1B and Whrn have been previously shown individually to play a crucial role in the cytoskeletal organization of myelinated axons in the PNS and CNS. Thus, ablation of *4.1B* alone led to destabilization of axonal domains along myelinated fibers, manifested by broken and stretched paranodal Caspr1, together with improperly localized and diffuse distribution of juxtaparanodal potassium channel $K_V1.1$, as revealed by immunostaining (Buttermore et al., 2011). *Whrn* mutant mice displayed paranodal decompaction phenotype established early on and progressed as animals aged (Green et al., 2013). Moreover, ablation of both proteins led to axonal pathology and formation of swellings containing mitochondria and vesicles in the cerebellum (Green et al., 2013). To further evaluate whether 4.1B and Whrn play a cooperative role in axonal domain organization and maintenance, we performed immunostaining analysis of cerebellar white matter tracts with antibodies against nodal βIV Spectrin, paranodal Caspr1 and juxtaparanodal $K_V1.2$ proteins in 2- and 6-month-old (mo) wild type, *4.1B* and *Whrn* single and double mutants (Fig. 2). As expected, the 2-month old control myelinated fibers showed well clustered nodal and juxtaparanodal domains separated by compact paranodes (Fig. 2 A-A'"). In 2-month old *4.1B* single mutants nodal βIV Spectrin was not disrupted, and only 15.43% of Caspr1 positive paranodes were showing structural abnormalities; however juxtaparanodal localization of $K_V1.2$ was significantly affected, resulting in diffuse staining in 50.77% of the juxtaparanodes (Fig. 2 B-B'", white arrowheads, J, K). In agreement with our previous reports, age matched *Whrn* knockout mice displayed onset of paranodal decompaction phenotype (15.83% of paranodes), as well as 38.08% of juxtaparanodes showing diffusion along myelinated fibers; notable changes were not observed in nodal areas (Fig. 2 C-C'", yellow arrowheads, J, K). Evaluation of white matter tracts from 2-month old *4.1B* and *Whrn* double mutants (*dKO*) revealed enhanced combined axonal phenotypes with diffuse and mislocalized $K_V1.2$ distribution in

62.44% of juxtaparanodes (white arrowheads; Fig. 2 D", D'", K) together with 37.75% of disrupted Caspr1-positive paranodal regions (Fig. 2 D', D'", yellow arrowheads, J).

To further determine whether phenotypes observed in younger mutants progressed towards more severity in older mutants, we performed similar immunostaining in 6-month old control and mutants. As expected, control myelinated fibers showed well preserved nodal, paranodal and juxtaparanodal areas along cerebellar white matter tracts (Fig. 2 E-E'"). However, evaluation of 6-month old *4.1B* single mutants revealed disrupted Caspr1 immunostaining in 26.04% of paranodes (Fig. 2 F', F'", red arrowheads, J). Moreover, the diffuse distribution of juxtaparanodal $K_V1.2$ seen at 2 months significantly progressed towards 67.62%, showing grainy staining along the length of the axon (Fig. 2 F"-F"', white arrowheads, K). Similarly, advanced paranodal despiralization phenotype observed with Caspr1 immunostaining in 6-month old *WKO* mutants showed long coiled threads outstretched outside of the paranodal region and invading the juxtaparanodal areas in 23.6% of paranodal population (Fig. 2 G', G'", yellow arrowheads, J). Consequently, in 62.27% of juxtaparanodes $K_V1.2$ moved towards the paranodal region, surrounding the nodal βIV Spectrin staining indicative of paranodal disorganization or showed diffuse distribution (Fig. 2 G'-G'", red asterisks, K). Significantly severe morphology of myelinated axons was observed in 6- month old cerebellar white matter of *dKO* mice. In most instances, no preserved paranodes or juxtaparanodes were detected with 61.23% of paranodes failing to flank the nodes showing long breaking gaps within Caspr1-positive immunostaining (Fig. 2 H', H''', J). In 85.59% of juxtaparanodes $K_V1.2$ pattern was similar to that observed in 6-month old *4.1B* single mutants with enhanced patchy and diffuse staining along the nerve fibers (Fig. 2 H'', H''', K). Overall, axonal domain disorganization phenotypes were significantly dependent on the genotype [($F(3,16)=15.78$; n=3; $P<0.0001$ for paranodes; $F(3,16)=90.97$; n=3; $P<0.0001$ for juxtaparanodes)] and age [($F(1,16) = 7.16$; n=3; $P=0.0166$ for paranodes; $F(1,16)=54.79$; n=3; $P<0.0001$ for juxtaparanodes)].

To further evaluate if 4.1B or Whrn regulate paranodal or juxtaparanodal protein levels, we performed immunoblot analysis of cerebellar lysates from *wt, 4.1B KO* and *WKO* single and double mutants. Analysis of paranodal Caspr1 [$F (3,16) = 0.08$; n=3; $P = 0.97$] (Fig. 3 A, B), NF186 [$F (3,16) = 0.68$; n=3; $P = 0.58$] and NF155 (NFCt) [$F (3,16) = 0.01$; n=3; $P = 1.00$] (Fig. 3 C, D) and juxtaparanodal Caspr2 [$F (3,16) = 0.05$; n=3; $P = 0.98$] (Fig. 3 E, F) and K/1.2 [$F (3,16) = 0.54$; n=3; $P = 0.66$] (Fig. 3 G, H), did not show any changes in their respective protein levels. Together, our data suggest that both 4.1B and Whrn, as axonal cytoskeletal proteins, ensure proper maintenance of the paranodal and juxtaparanodal domains and preservation of the architecture of the cerebellar myelinated axons.

Absence of Band 4.1B and Whrn Affects the Ultrastructural Organization of Myelinated Axons

Since our immunostaining data revealed progressive destabilization of paranodes and juxtaparanodes in 4.*1B* and *Whrn* single and double mutants, our next step was to evaluate the impact of combined loss of 4.1B and Whrn on the ultrastructural organization of axonal domains in the cerebellar white matter. Previous studies have reported that loss of 4.1B led to disorganization of axo-glial junctions (AGJs) in the spinal cord and sciatic nerve

myelinated fibers, which resulted in myelin loop detachment from the axolemma, and loss of electron densities (Buttermore et al., 2011). Moreover, *Whrn* ablation led to disruptive consequences on the ultrastructural organization of myelinated nerve fibers, which manifested by weakly defined AGJs, disorganized neurofilaments and microtubules, with accumulation of lipid vesicles and mitochondria in the paranodal region (Green et al., 2013). In order to evaluate the role of both cytoskeletal proteins in axonal ultrastructure organization, we proceeded with longitudinal sections of two and six month old control, *4.1B* and *Whrn* single and double mutants. High magnification images of longitudinal sections from 2-month old control animals revealed intact myelin loops properly attached to axolemma with evenly spaced AGJ electron densities (Fig. 4 A, blue arrowheads). In age matched *4.1B KO* mice signs of paranodal destabilization were observed. The myelin loop proximal to the nodal region was detached from the axolemma (Fig. 4B, black arrow). Moreover, numerous cases of everted paranodal loops were observed (Fig. 4B, red asterisks) together with cases of alternating stretches of poorly defined or preserved septa (Fig. 4B, black and blue arrowheads, respectively). Similarly, 2-month old *WKO* single mutants displayed paranodal abnormalities, manifested by loss of AGJs (Fig. 4D, black arrowheads). Additionally, in *WKO* mice we observed organelle accumulations in the paranodal area (Fig. 4D, red arrowheads) and at the paranodal loops (Fig. 4D, blue asterisks). Assessment of longitudinal EM sections in 2-month old *dKO* animals revealed combination of phenotypes from single knockout mice: fuzzy AGJs, detached and disconnected myelin loops from the axonal membrane (Fig. 4F, black arrow), and accumulation of organelles (Fig. 4F, red arrowhead).

Next, we evaluated the ultrastructure of axonal domains in cerebellar myelinated fibers from 6-month-old *wt, 4.1B KO, WKO* and *dKO* animals. As expected in control samples, we observed properly aligned paranodal loops flanking the nodal area from both sides and connected to axolemma through the AGSJs (Fig. 4H). In the single *4.1B KO* mice progression of the AGJs destabilization was observed. If at 2 months, partial presence of AGJs was still observed at the paranodes, four months later everted paranodal loops (Fig. 4 I, red asterisks) and myelin loops with longer stretches of no detectable electron dense septa were observed (Fig. 4 C and I, black arrowheads). Loss of Whrn led to further advancement in disrupted axonal ultrastructural phenotype in 6-month old *WKO* animals, displayed by eversion of paranodal myelin loops (Fig. 4 E, red asterisks and J), missing AGJs (Fig. 4 E, black arrowheads), excess myelin waviness in paranodal region (Fig. 4 J, blue arrows) and large organelle accumulations (Fig. 4 E, J, red arrowheads). Enhanced disorganization of paranodal myelin loops was observed in *dKO* mutants, compared to other mutant genotypes. Thus, by 6 months long segments of paranodal region were extremely detached from the axolemma forming large gaps in between the myelin loops and axonal membrane (Fig. 4 G, K, black arrows). Moreover, severe phenotypes with everted or wavy paranodal loops, lack of AGJs (Fig. 4 G, black arrowheads) and accumulation of mitochondria were readily observed in *dKO* animals (Fig. 4 G, K). These data demonstrate that both 4.1B and Whrn functioning as cytoskeletal scaffolding proteins are essential for preserving the ultrastructural organization of axonal domains in myelinated fibers.

Loss of 4.1B and Whrn Causes Formation of Swellings in Purkinje Neuron Axons

Purkinje neurons are the largest neurons in the brain and the sole output source from the cerebellum with very small diameter myelinated axons. The health of the Purkinje neurons is central for proper motor performance. Since our results distinctively showed disorganization of axonal domains in the cerebellar white matter tracts followed by single or double loss of 4.1B and Whrn, we aimed to assess overall gross morphology of the cerebellum in 6mo control, single *4.1BKO* and WKO, as well as *dKO* mice. After immunostaining with anti-calbindin antibodies, we examined overall anatomy of layer arrangement in lobule VIa of the cerebellum. There were no substantial differences in the size of lobule Via or the cerebellar layers, and all genotypes displayed properly formed molecular, Purkinje cell and granule cell layers (Fig. 5 A-D). Our quantifications revealed no significant differences in interneurons number (159±58.89, 137.5±4.33, 152.5±38.97 and 126±13.51 interneurons/lobule in *wt, 4.1B KO, WKO* and *dKO*, respectively ([F (3,8) = 0.34; n=3; P = 0.797], one-way ANOVA with Bonferroni's post-hoc analysis) and only slight decrease in Purkinje cells in the *dKO* mice (62±3.46, 63±15.59, 53.5±2.60 and 47±0.97 Purkinje neurons/lobule in *wt, 4.1B KO, WKO* and *dKO*, respectively ([F (3,8) = 1.74; n=3; P = 0.235], one-way ANOVA with Bonferroni's post-hoc analysis). Even though there were no distinctive differences in the cerebellar gross morphology, we noticed presence of swellings along the Purkinje axons in 6mo single *4.1B KO* and *WKO*, and their increased number in the *dKO* mice (Fig. 5 B-D compared to A, swellings marked with white arrowheads).

Formation of swellings along myelinated fibers is a hallmark of altered axonal transport, which is highly dependent on intact cytoskeleton. Disrupted cytoskeleton, accompanied with misoriented microtubules and neurofilaments, leads to changes in cellular organelles and protein transport, and their aggregated accumulation along the axons (Garcia-Fresco et al., 2006; Pillai et al., 2007; Saifetiarova et al., 2017a). Interestingly, we found a greater number of axonal swellings were formed in *dKO* animals, compared to single *4.1B KO and WKO* mice, suggesting more severely affected axonal transport in those animals (Fig. 5 B compared to C and D, O). In order to see if the swellings formation along Purkinje axons occurs early on, we performed immunostaining of 2mo cerebellum slices from control, single and double mutant animals. Our results indicate, that, indeed, axonal swellings formation occurs much earlier, as 2mo *4.1B KO* and *dKO* animals already displayed bead-like aggregates along Purkinje myelinated fibers, with rarely occurring swellings in *WKO* mutants and normal healthy axons in control mice (Fig. 5 O). However, by 6mo swellings in *4.1B KO* and *dKO* mutants become larger, and *WKO* mutants start to display axonal aggregates more often (Fig. 5 N, O). The size of the axonal swellings and density were both affected by genotype [(F(3,16)=10.55, n=3, P=0.0005 for size; (F(3,16)=16.24, n=3, P<0.0001 for density)] and age [(F(1,16)=163.93, n=3, P<0.0001 for size; (F(1,16)=11.23, n=3, P=0.0041 for density)]. Additional immunostaining with antibodies against Caspr1 and Neurofilament has shown that in agreement with our previous studies (Pillai et al., 2007), observed swellings were below the Caspr1 positive paranodal staining, occupying the first paranodal segment (Fig. 5 I, J, K) or residing in-between two paranodes (Fig. 5 I, K). We observed Neurofilament positive immunostaining within the swellings, which was mostly prominent in *dKO* mice (Fig. 5 F, J, K). Interestingly, we also noticed accumulation of

Caspr1 in the swellings of the *dKO* animals, suggesting that proteins that are being trafficked from the soma to corresponding axonal domains are accumulating within the swellings due to axonal transport defects (Fig. 5 K, L). Western blot analysis of cerebellar lysates has shown slight but not statistically significant upregulation of the Neurofilament in the *dKO* mice (1.77±0.55 and 2.18±1.11 times in 2 and 6mo *dKO* respectively, compared to corresponding control values) (Fig. 5 M), which can be a compensatory reaction of the neurons due to disorganization of the cytoskeletal structure of the axons. Thus, our data indicate that 4.1B and Whrn help preserve the axonal health of Purkinje axons, and their loss leads to potential axonal transport defects manifested in young *4.1B KO, WKO and dKO* mice as bead-like aggregates, with further increase in their size with age, as accumulation of cytoskeletal components and axonal domain proteins builds up inside these swellings.

Ablation of 4.1B and Whirlin Results in Axonal Cytoskeletal Disorganization and Pathology

Since our immunostaining data revealed swellings along Purkinje axons in *4.1B KO, WKO and dKO* animals, we decided to look at higher magnification of the axonal cytoskeletal ultrastructure and the content of swellings in 6mo animals in longitudinal sections. As expected, axons in control samples were displaying an intact myelin sheath in tight apposition with the axonal membrane, normal organization of microtubules and neurofilaments, no accumulations of membranous organelles or any other pathology (Fig. 6A). A detailed assessment of myelinated fibers in 6mo *4.1B KO* mice revealed various axonal pathologies (Fig. 6 B-D, K-L). First, accumulation of smooth endoplasmic reticulum (SER) and mitochondria was observed along the axons, as well as in the axonal swellings (Fig. 6 B, red arrow, L). Some of the axonal mitochondria were electron dense displaying signs of mitochondrial pathology (Fig. 6 K, blue arrows). Additionally, there were extended areas of myelin detached from the axolemma around the swellings (Fig. 6 C, blue arrows). The cytoskeletal organization of *4.1B KO* axons was altered, which manifested by either abnormal aggregation of neurofilaments within axonal cytoplasm (Fig. 6 B, black arrows) or significantly reduced density of cytoskeletal components (Fig. 6 D). Occasionally, myelin inclusions were detected along the axons (Fig. 6 D, red arrowheads).

Similar to *4.1B KO* mice, 6 mo *WKO* animals revealed accumulation of SER in axonal swellings (Fig. 6 G, red arrowheads, N), detachment of axolemma from the myelin (Fig. 6 E, blue arrowheads), as well as abnormal aggregation of the neurofilaments (especially in the paranodal and juxtaparanodal regions, Fig. 6 F, black arrowheads) and decreased density of cytoskeletal structures (Fig. 6 E). However, additionally we noticed accumulation of large transport vesicles along the axons and inside the swellings (Fig. 6 E, M, N, red asterisks). Ultrastructural analysis of myelinated axons from *dKO* mice revealed prominent disorganization of cytoskeleton and potential axonal transport alterations (Fig. 6 H-P). The most striking phenotypes observed were: extensive accumulations of transport vesicles along the axons (Fig. 6 H, red asterisks), accumulations of electron dense mitochondria in the paranodal area (Fig. 6 I, red arrowheads), as well as loss of cytoskeletal ultrastructure with accumulation of membranous aggregates (Fig. 6 J, red arrowheads). Overall, the ultrastructural analysis of the myelinated axons revealed that both 4.1B and Whrn are required for proper organization of the cytoskeletal components and to preserve the axonal cytoskeletal ultrastructure, and that their absence results in axonal transport defects leading

to accumulation of membranous organelles, transport vesicles and neurofilament aggregation.

Loss of 4.1B and Whrn Progressively Affects Locomotion

One of the main functions of the cerebellum is to coordinate precise locomotor activity. Impaired cerebellar functions result in loss of equilibrium, irregular ataxic gait, errors in the direction, speed and magnitude of movements. Since our data showed altered cerebellar morphology reflected as molecular disorganization of axonal domains, impaired cytoskeletal ultrastructure of myelinated fibers, as well as swollen Purkinje axons, we aimed to assess, how these alterations affected cerebellum-dependent locomotor functions. We used Catwalk – an automated gait analysis system in order to collect gait parameters from 2 and 6-month-old *wt, 4.1B KO, WKO* and *dKO* mice (representative footprints are depicted on Fig. 7 A). *4.1B/Whrn* double mutants showed altered foot print patterns which is a sign of cerebellar ataxia (Buttermore et al., 2012). According to this analysis, there were no major changes in average running speed [$F(3,40) = 0.34$; n=5-7; $P = 0.79$] (Fig. 7 B), as well as in the regularity index [$F(3,40) = 0.75$; n=5-7; $P = 0.53$] (% of regular step patterns, Fig. 7 C) between genotypes of both ages. Base of support estimation (distance between two front or hind paws, measured perpendicular to walking direction) revealed its consistent but not statistically significant reduction for hind paws in 2 and 6 mo *dKO* mice [$F(3,40) = 0.56$; n=5-7; $P = 0.65$ for front paws and $F(3,40) = 0.06$; n=5-7; $P = 0.98$ for hind paws] (Fig. 7 D, E). Mean intensity of the paw placement (mean intensity of the pixels forming the maximum area) was reduced for front paws between 2 and 6 mo *WKO* ($P<0.01$) and *dKO* ($P<0.01$) mice [$F(3,40) = 0.87$; n=5-7; $P = 0.46$] (Fig. 7 F, G). The same parameter for the hind paws was reduced between 2 and 6 mo *4.1B KO* ($P<0.001$), *WKO* ($P<0.01$), as well as *dKO* ($P<0.001$) mice, and was significantly lower in 6 mo *4.1B KO* animals compared to the same age control group($P<0.05$) [$F(3,40) = 5.69$; n=5-7; $P = 0.0024$] (Fig. 7 H). These data suggest that with the loss of 4.1B and Whrn animals are not able to place their weight properly on the front or hind limbs. Considering that one of the gait compensatory mechanisms of cerebellar ataxic gait is steps shortening and shuffling (Stolze et al., 2002), we assessed stride length in all genotypes. This analysis showed that at 2 mo there is no change between groups, however at 6 mo in *4.1B KO* and *dKO* mice for both front and hind paws the stride length is slightly reduced [$F(3,40) = 1.36$; n=5-7; $P = 0.27$] (Fig. 7 I, J) compared to same genotype 2 mo group or same age control animals. As a result of the shortening stride the cadence (steps/second) values were elevated in *4.1B KO* and *dKO* mice at 6 mo suggesting establishment of a shuffling phenotype (10.97±0.80; 14.50±1.49; 11.23±1.66 and 14.19±2.23 steps/s in *wt, 4.1B KO, WKO* and *dKO*. [$F(3,8) = 2.67$; n=5-7; $P = 0.12$], one-way ANOVA with Bonferroni's post-hoc analysis). Together, these data reveal that loss of 4.1 B and Whrn changes the animals gait parameters, affecting their ability to fully apply their weight on their limbs, leading to reduction of stride length and increased cadence, which is consistent with progressive cerebellar dysfunction.

DISCUSSION

The cellular cytoskeleton plays an important role in providing structural strength to the cytoplasm and also in scaffolding key molecules to assemble membrane associated

complexes. These complexes also serve as signal transduction centers that allow changes in cell behavior and differentiation. Axonal cytoskeletal scaffolding proteins connect with membrane complexes at unique molecular domains as well as along the axon. The cytoskeletal scaffolding protein 4.1B and Whrn have been shown to assemble protein complexes at multiple locations in the nervous system. Yet their collective functions in the myelinated axons have remained to be established. Here we show that both these proteins are also critically required for proper paranodal axonal domain maintenance and also overall axonal health. Thus, combined loss of both these proteins leads to severe ultrastructural changes that affect not only at the axonal domains but also at the axonal transport and general architecture level, eventually leading to axonal degeneration.

Band 4.1B and Whrn: Scaffolding Functions in Axonal Domains

The organization of specialized membrane-associated complexes allows a unique assembly of molecules that interact with the cytoplasmic regions of transmembrane proteins and structurally link them with the cellular cytoskeleton for both the physical integrity and also for signal transduction processes. The Band 4.1 family members have emerged as cytoskeletal scaffolding proteins that are expressed in blood cells, epithelial cells and neurons (Cohen and Foley, 1982; Conboy, 1993; Hoover and Bryant, 2000; Sun et al., 2002; Chen et al., 2005; Ohara et al., 2000).). Band 4.1B is mostly expressed in the nervous system with specific localization at the paranodes, juxtaparanodes and the internodal areas (Horresh et al., 2010; Buttermore et al., 2011; Einheber et al., 2012; Cifuentes-Diaz et al., 2012). At the paranodes and juxtaparanodes, 4.1B interacts with Caspr1 and Caspr2, respectively, and its loss affected the localization of the juxtaparanodal and paranodal complexes (Buttermore et al., 2011; Horresh et al., 2010). While the initial localization of these proteins is relatively less affected, older 4.1B mutants show significant disorganization of the paranodal and juxtaparanodal regions with loss of axo-glial septa at the paranodes eventually leading to paranodal disorganization (Buttermore et al., 2011). Whrn, on the other hand, is a PDZ domain and a proline rich region containing scaffolding protein that is essential for visual and auditory function (Yang et al., 2010). According to an RNA-Seq transcriptome and splicing database of glia, neurons, and vascular cells of the cerebral cortex, Whrn is mainly expressed in neurons, astrocytes and microglia. Its expression in myelinating oligodendrocytes is comparatively low (FPKM<2) (Zhang et al., 2014). Surprisingly, loss of Whrn does not affect the localization of Caspr1 or Caspr2 but affects the compaction of the paranodal loops, which spring out loosely at the paranodes (Green et al., 2013). In *4.1B* mutants occasionally such phenotype is also observed but not to a degree that resembles *Whrn* mutants (Green et al., 2013). Since Caspr1 and Caspr2 interact with 4.1B (Buttermore et al., 2011), and 4.1B may indirectly interact with Whrn via p55 (Okumura et al., 2010), it remained unresolved as to how 4.1B and Whrn complex function together in the myelinated axons to preserve axonal domains and axonal cytoskeleton. Loss of both these proteins affects axonal cytoskeleton as axonal transport is disrupted and myelinated axons accumulate organelles and form large swelling that are filled with neurofilaments, SER lattice and other axonal organelles. The paranodal areas often show severe disorganization with myelin loop eversion that is generally observed in paranodal mutants (Bhat et al., 2001; Boyle et al., 2001; Pillai et al., 2009). Thus, biochemical interactions between Caspr1/2, 4.1B and Whrn may assemble unique molecular complexes at the paranodal/juxtaparanodal

areas and along the internode that ensures proper cytoskeletal organization to preserve the structural integrity of myelinated axon.

Cytoskeletal Disorganization and Axonal Swellings

Proper cytoskeletal organization is essential to maintain structural and functional basis of myelinated axons, as well as it is required to ensure proper transport of proteins synthesized in soma to other specific neuronal compartments along the axon. Axonal transport provides neuronal fibers and nerve terminals with lipids and proteins, as well as eliminates misfolded proteins (Millecamps and Julien, 2013; Perlson et al., 2010). Disruption of the cytoskeletal organization leads to formation of toxic aggregates along the axons, which contain mitochondria, degraded membranous organelles and cytoskeletal components, such as neurofilaments. Defects in transport lead to diminished functionality of the axons, their degeneration and neuronal cell death. This has been observed in various neurological disorders, such as Charcot-Marie-Tooth neuropathy (Brownlees et al., 2002; Misko et al., 2010), amyotrophic lateral sclerosis (Ilieva et al., 2009; Ligon et al., 2005), Parkinson's (Abou-Sleiman et al., 2006; Saha et al., 2004) and Huntington's disease (McGuire et al., 2006; Morfini et al., 2009), Alzheimer's disease and other dementias (Kamal et al., 2001; Morfini et al., 2007).

The maintenance of axonal domain organization and preservation of axonal health requires intact axonal cytoskeleton. Each axonal domain along myelinated fiber contains unique molecular complexes of transmembrane proteins which are anchored to axonal cytoskeleton by scaffolding proteins. Thus, protein 4.1B through its interaction with Caspr1 at the paranode, Caspr2 in the juxtaparanode (Buttermore et al., 2011) and Nectin-like protein family at the internodal area (Maurel et al., 2007) provides intact organization of these domains. Loss of 4.1B leads to disorganization of paranodal and juxtaparanodal regions with subsequent evidences of axonal transport defects, such as formation of axonal swellings. Band 4.1B is an ERM (ezrin/radixin/moesin) domain containing protein, which is known to be a binding site for PDZ proteins. Whrn has been identified as a novel PDZ protein (Mburu et al., 2003) and it indirectly may interact with 4.1B through the membrane-associated guanylate kinase protein p55 in the inner ear hair cells (Okumura et al., 2010). Despite not being able to co-localize all three proteins (4.1B, Whrn and p55) in the cerebellum, 4.1B and Whrn were detected in the myelinated fibers, suggesting their cooperative role in the white matter cerebellar tracts. Moreover, we observed their mutual effect on each other's localization in molecular, Purkinje cell and granule layers, but not in the white matter axonal tracts. Such differences could be potentially regulated at the post-transcriptional level where protein distribution throughout different cell compartments might be differentially affected. Most likely, Whrn binds to 4.1B, the way PDZ proteins bind ERM family proteins, to stabilize and link transmembrane proteins to the actin cytoskeleton (Lue et al., 1994; Reczek et al., 1997). Our data indicates that elimination of both proteins disrupts paranodal and juxtaparanodal organization of myelinated fibers more severely than single ablation of proteins, leading to enhanced axonal pathology. It is known that axonal transport defects and axonal swellings are the hallmark of axonal injury which accompanies various chronical neurological disorders (Beirowski et al., 2010). Disorders that are accompanied with axonal swellings include multiple sclerosis (Ferguson et al., 1997; Trapp et al., 1998), traumatic

brain injury (Cheng and Povlishock, 1988), Alzheimer's (Tsai et al., 2004) and Parkinson's disease (Galvin et al., 1999), Creutzfeldt-Jakob disease (Liberski and Budka, 1999), HIV dementia (Adle-Biassette et al., 1999). Formation of axonal swellings has shown association with decline in cognition, behavior, motor and sensory skills (Beirowski et al., 2010). In our studies, we noticed increased number of axonal swellings in the *dKO* animals with neurofilamentous masses and paranodal Caspr1 accumulations. This is an indication of significant axonal transport defects, where proteins synthesized in neuronal soma fail to be delivered and localized to the destined axonal compartments. Formation of axonal swellings in *4.1B* and *WKO* single and double knockout animals is in agreement with previous observations, where disruption of axo-glial junction led to cytoskeletal disorganization and axonal degeneration in *Caspr1* and *CGT* knockout mice (Garcia-Fresco et al., 2006). Thus, our data indicate that *4.1B* and *Whrn* play a complex role in maintaining the integrity of the axonal domains and the paranodal septate junctions, and that combined loss of 4.1B/Whrn leads to enhanced destabilization of the axonal cytoskeleton and formation of swellings and further destabilization of the molecular complexes at axonal domains. These phenotypes suggest that these proteins play interdependent roles in myelinated axons.

Cytoskeletal Scaffolding Proteins and Neurological Disorders

The function of Whrn was previously associated with the auditory and vision system, since numerous human *WHRN* mutations are associated with the Usher syndrome (Grati et al., 2012; van Wijk et al., 2006). In the visual system, the long isoform of Whrn is expressed in the retina and mediates formation of the multi-protein complex with Usherin and VLGR1(Yang et al., 2010). Both long and short isoforms of Whrn are expressed in the ear but the short isoform is more important in the auditory system, as mutations in the short isoform are correlated with more significant hearing impairment than mutations in the long isoform (Yang et al., 2010). 4.1B as such has not been associated with any neurological deficits but has been identified as a tumor suppressor gene (Singh et al., 2004). In myelinated axons, the cytoskeletal scaffolding proteins are indispensable components of axonal domains. The voltage gated sodium channels at the nodes of Ranvier are stabilized by cytoskeletal scaffolding proteins Ankyrin G and βIV Spectrin (Ho et al., 2014; Komada and Soriano, 2002; Saifetiarova et al., 2017b), the paranodal components of the axo-glial junctions are stabilized through 4.1B, Ankyrin B and βII Spectrin (Horresh et al., 2010), and finally juxtaparanodal components are linked to the actin cytoskeleton through their interaction with protein 4.1B (Buttermore et al., 2011). Thus, cytoskeletal scaffolding proteins are the critical elements in allowing organization of large molecular complexes at unique axonal domains, and any disruption in this scaffolding ability leads to abnormalities in axons or cellular cytoskeleton. Our studies described here provide evidence that Whrn and 4.1B play cooperative roles at the paranodes and juxtaparanodes to stabilize these domains and also to maintain proper axonal cytoskeleton. Our studies further suggest novel neuronal functions of Whrn for long-term axonal health and possibility of neuronal complications in patients with *WHRN* mutations. Even though there are no 4.1B human linked neurological disorders, mutations of its binding partners Caspr1 (*CNTNAP1*) and Caspr2 (*CNTNAP2*) have been implicated in arthrogryposis multiplex congenital (Laquerriere et al., 2014) and autism spectrum disorders (Arking et al., 2008), respectively, further highlighting their role in neuronal function.

Acknowledgements

We thank members of the Bhat Laboratory for valuable suggestions and many helpful discussions. The electron microscopic analysis of tissues was performed at the UT Health EM Facility.

Grant Support

This work was supported by grants from NIH NIGMS GM063074, National Multiple Sclerosis Society, the Zachry Foundation, the Morrison Trust and the Owen's Foundation.

REFERENCES

Abou-Sleiman PM, Muqit MM, and Wood NW (2006). Expanding insights of mitochondrial dysfunction in Parkinson's disease. Nat Rev Neurosci 7, 207–219. [PubMed: 16495942]

Adle-Biassette H, Chretien F, Wingertsmann L, Hery C, Ereau T, Scaravilli F, Tardieu M, and Gray F (1999). Neuronal apoptosis does not correlate with dementia in HIV infection but is related to microglial activation and axonal damage. Neuropathol Appl Neurobiol 25, 123–133. [PubMed: 10216000]

Arking DE, Cutler DJ, Brune CW, Teslovich TM, West K, Ikeda M, Rea A, Guy M, Lin S, Cook EH, et al. (2008). A common genetic variant in the neurexin superfamily member CNTNAP2 increases familial risk of autism. Am J Hum Genet 82, 160–164. [PubMed: 18179894]

Beirowski B, Nogradi A, Babetto E, Garcia-Alias G, and Coleman MP (2010). Mechanisms of axonal spheroid formation in central nervous system Wallerian degeneration. J Neuropathol Exp Neurol 69, 455–472. [PubMed: 20418780]

Bhat MA, Rios JC, Lu Y, Garcia-Fresco GP, Ching W, St Martin M, Li J, Einheber S, Chesler M, Rosenbluth J, et al. (2001). Axon-glia interactions and the domain organization of myelinated axons requires neurexin IV/Caspr/Paranodin. Neuron 30, 369–383. [PubMed: 11395000]

Brownlees J, Ackerley S, Grierson AJ, Jacobsen NJ, Shea K, Anderton BH, Leigh PN, Shaw CE, and Miller CC (2002). Charcot-Marie-Tooth disease neurofilament mutations disrupt neurofilament assembly and axonal transport. Human molecular genetics 11, 2837–2844. [PubMed: 12393795]

Buttermore ED, Dupree JL, Cheng J, An X, Tessarollo L, and Bhat MA (2011). The cytoskeletal adaptor protein band 4.1B is required for the maintenance of paranodal axoglial septate junctions in myelinated axons. J Neurosci 31, 8013–8024. [PubMed: 21632923]

Cheng CL, and Povlishock JT (1988). The effect of traumatic brain injury on the visual system: a morphologic characterization of reactive axonal change. J Neurotrauma 5, 47–60. [PubMed: 3193463]

Cifuentes-Diaz C, Chareyre F, Garcia M, Devaux J, Carnaud M, Levasseur G, Niwa-Kawakita M, Harroch S, Girault JA, Giovannini M, et al. (2011). Protein 4.1B contributes to the organization of peripheral myelinated axons. PLoS One 6, e25043. [PubMed: 21966409]

Denisenko-Nehrbass N, Oguievetskaia K, Goutebroze L, Galvez T, Yamakawa H, Ohara O, Carnaud M, and Girault JA (2003). Protein 4.1B associates with both Caspr/paranodin and Caspr2 at paranodes and juxtaparanodes of myelinated fibres. Eur J Neurosci 17, 411–416. [PubMed: 12542678]

Einheber S, Meng X, Rubin M, Lam I, Mohandas N, An X, Shrager P, Kissil J, Maurel P, and Salzer JL (2013). The 4.1B cytoskeletal protein regulates the domain organization and sheath thickness of myelinated axons. Glia 61, 240–253. [PubMed: 23109359]

Ferguson B, Matyszak MK, Esiri MM, and Perry VH (1997). Axonal damage in acute multiple sclerosis lesions. Brain 120 (Pt 3), 393–399. [PubMed: 9126051]

Friedman TB, Schultz JM, Ahmed ZM, Tsilou ET, and Brewer CC (2011). Usher syndrome: hearing loss with vision loss. Adv Otorhinolaryngol 70, 56–65. [PubMed: 21358186]

Galvin JE, Uryu K, Lee VM, and Trojanowski JQ (1999). Axon pathology in Parkinson's disease and Lewy body dementia hippocampus contains alpha-, beta-, and gamma-synuclein. Proc Natl Acad Sci U S A 96, 13450–13455. [PubMed: 10557341]

Garcia-Fresco GP, Sousa AD, Pillai AM, Moy SS, Crawley JN, Tessarollo L, Dupree JL, and Bhat MA (2006). Disruption of axo-glial junctions causes cytoskeletal disorganization and degeneration of Purkinje neuron axons. Proc Natl Acad Sci U S A 103, 5137–5142. [PubMed: 16551741]

Grati M, Shin JB, Weston MD, Green J, Bhat MA, Gillespie PG, and Kachar B (2012). Localization of PDZD7 to the stereocilia ankle-link associates this scaffolding protein with the Usher syndrome protein network. J Neurosci 32, 14288–14293. [PubMed: 23055499]

Green JA, Yang J, Grati M, Kachar B, and Bhat MA (2013). Whirlin, a cytoskeletal scaffolding protein, stabilizes the paranodal region and axonal cytoskeleton in myelinated axons. BMC Neurosci 14, 96. [PubMed: 24011083]

Hamers FP, Lankhorst AJ, van Laar TJ, Veldhuis WB, and Gispen WH (2001). Automated quantitative gait analysis during overground locomotion in the rat: its application to spinal cord contusion and transection injuries. J Neurotrauma 18, 187–201. [PubMed: 11229711]

Ho TS, Zollinger DR, Chang KJ, Xu M, Cooper EC, Stankewich MC, Bennett V, and Rasband MN A hierarchy of ankyrin-spectrin complexes clusters sodium channels at nodes of Ranvier. Nat Neurosci.

Ho TS, Zollinger DR, Chang KJ, Xu M, Cooper EC, Stankewich MC, Bennett V, and Rasband MN (2014). A hierarchy of ankyrin-spectrin complexes clusters sodium channels at nodes of Ranvier. Nat Neurosci 17, 1664–1672. [PubMed: 25362473]

Horresh I, Bar V, Kissil JL, and Peles E (2010). Organization of myelinated axons by Caspr and Caspr2 requires the cytoskeletal adapter protein 4.1B. J Neurosci 30, 2480–2489. [PubMed: 20164332]

Ilieva H, Polymenidou M, and Cleveland DW (2009). Non-cell autonomous toxicity in neurodegenerative disorders: ALS and beyond. J Cell Biol 187, 761–772. [PubMed: 19951898]

Kamal A, Almenar-Queralt A, LeBlanc JF, Roberts EA, and Goldstein LS (2001). Kinesin-mediated axonal transport of a membrane compartment containing beta-secretase and presenilin-1 requires APP. Nature 414, 643–648. [PubMed: 11740561]

Kevenaar JT, and Hoogenraad CC (2015). The axonal cytoskeleton: from organization to function. Front Mol Neurosci 8, 44. [PubMed: 26321907]

Komada M, and Soriano P (2002). [Beta]IV-spectrin regulates sodium channel clustering through ankyrin-G at axon initial segments and nodes of Ranvier. J Cell Biol 156, 337–348. [PubMed: 11807096]

Laquerriere A, Maluenda J, Camus A, Fontenas L, Dieterich K, Nolent F, Zhou J, Monnier N, Latour P, Gentil, D_V et al. (2014). Mutations in CNTNAP1 and ADCY6 are responsible for severe arthrogryposis multiplex congenita with axoglial defects. Human molecular genetics 23, 2279–2289. [PubMed: 24319099] $_V$

Liberski PP, and Budka H (1999). Neuroaxonal pathology in Creutzfeldt-Jakob disease. Acta Neuropathol 97, 329–334. [PubMed: 10208271]

Ligon LA, LaMonte BH, Wallace KE, Weber N, Kalb RG, and Holzbaur EL (2005). Mutant superoxide dismutase disrupts cytoplasmic dynein in motor neurons. Neuroreport 16, 533–536. [PubMed: 15812301]

Lue RA, Marfatia SM, Branton D, and Chishti AH (1994). Cloning and characterization of hdlg: the human homologue of the Drosophila discs large tumor suppressor binds to protein 4.1. Proc Natl Acad Sci U S A 91, 9818–9822. [PubMed: 7937897]

Maurel P, Einheber S, Galinska J, Thaker P, Lam I, Rubin MB, Scherer SS, Murakami Y, Gutmann DH, and Salzer JL (2007). Nectin-like proteins mediate axon Schwann cell interactions along the internode and are essential for myelination. J Cell Biol 178, 861–874. [PubMed: 17724124]

Mburu P, Kikkawa Y, Townsend S, Romero R, Yonekawa H, and Brown SD (2006). Whirlin complexes with p55 at the stereocilia tip during hair cell development. Proc Natl Acad Sci U S A 103, 10973–10978. [PubMed: 16829577]

Mburu P, Mustapha M, Varela A, Weil D, El-Amraoui A, Holme RH, Rump A, Hardisty RE, Blanchard S, Coimbra RS, et al. (2003). Defects in whirlin, a PDZ domain molecule involved in stereocilia elongation, cause deafness in the whirler mouse and families with DFNB31. Nat Genet 34, 421–428. [PubMed: 12833159]

McGuire JR, Rong J, Li SH, and Li XJ (2006). Interaction of Huntingtin- associated protein-1 with kinesin light chain: implications in intracellular trafficking in neurons. The Journal of biological chemistry 281, 3552–3559. [PubMed: 16339760]

Millecamps S, and Julien JP (2013). Axonal transport deficits and neurodegenerative diseases. Nat Rev Neurosci 14, 161–176. [PubMed: 23361386]

Misko A, Jiang S, Wegorzewska I, Milbrandt J, and Baloh RH (2010). Mitofusin 2 is necessary for transport of axonal mitochondria and interacts with the Miro/Milton complex. J Neurosci 30, 4232–4240. [PubMed: 20335458]

Morfini G, Pigino G, Mizuno N, Kikkawa M, and Brady ST (2007). Tau binding to microtubules does not directly affect microtubule-based vesicle motility. J Neurosci Res 85, 2620–2630. [PubMed: 17265463]

Morfini GA, You YM, Pollema SL, Kaminska A, Liu K, Yoshioka K, Bjorkblom B, Coffey ET, Bagnato C, Han Dv et al. (2009). Pathogenic huntingtin inhibits fast axonal transport by activating JNK3 and phosphorylating kinesin. Nat Neurosci 12, 864–871. [PubMed: 19525941]

Okumura K, Mochizuki E, Yokohama M, Yamakawa H, Shitara H, Mburu P, Yonekawa H, Brown SD, and Kikkawa Y (2010). Protein 4.1 expression in the developing hair cells of the mouse inner ear. Brain Res 1307, 53–62. [PubMed: 19853587]

Parra M, Gascard P, Walensky LD, Gimm JA, Blackshaw S, Chan N, Takakuwa Y, Berger T, Lee G, Chasis JA, et al. (2000). Molecular and functional characterization of protein 4.1B, a novel member of the protein 4.1 family with high level, focal expression in brain. The Journal of biological chemistry 275, 3247–3255. [PubMed: 10652311]

Perlson E, Maday S, Fu MM, Moughamian AJ, and Holzbaur EL (2010). Retrograde axonal transport: pathways to cell death? Trends Neurosci 33, 335–344. [PubMed: 20434225]

Pillai AM, Garcia-Fresco GP, Sousa AD, Dupree JL, Philpot BD, and Bhat MA (2007). No effect of genetic deletion of contactin-associated protein (CASPR) on axonal orientation and synaptic plasticity. J Neurosci Res 85, 2318–2331. [PubMed: 17549747]

Reczek D, Berryman M, and Bretscher A (1997). Identification of EBP50: A PDZ- containing phosphoprotein that associates with members of the ezrin-radixin- moesin family. J Cell Biol 139, 169–179. [PubMed: 9314537]

Saha AR, Hill J, Utton MA, Asuni AA, Ackerley S, Grierson AJ, Miller CC, Davies AM, Buchman VL, Anderton BH, et al. (2004). Parkinson's disease alpha-synuclein mutations exhibit defective axonal transport in cultured neurons. J Cell Sci 117, 1017–1024. [PubMed: 14996933]

Saifetiarova J, Liu X, Taylor AM, Li J, and Bhat MA (2017a). Axonal domain disorganization in Caspr1 and Caspr2 mutant myelinated axons affects neuromuscular junction integrity, leading to muscle atrophy. J Neurosci Res 95, 1373–1390. [PubMed: 28370195]

Saifetiarova J, Taylor AM, and Bhat MA (2017b). Early and Late Loss of the Cytoskeletal Scaffolding Protein, Ankyrin G Reveals Its Role in Maturation and Maintenance of Nodes of Ranvier in Myelinated Axons. J Neurosci 37, 2524–2538. [PubMed: 28148727]

Singh V, Miranda TB, Jiang W, Frankel A, Roemer ME, Robb VA, Gutmann DH, Herschman HR, Clarke S, and Newsham IF (2004). DAL-1/4.1B tumor suppressor interacts with protein arginine N-methyltransferase 3 (PRMT3) and inhibits its ability to methylate substrates in vitro and in vivo. Oncogene 23, 7761–7771. [PubMed: 15334060]

Stolze H, Klebe S, Petersen G, Raethjen J, Wenzelburger R, Witt K, and Deuschl G (2002). Typical features of cerebellar ataxic gait. J Neurol Neurosurg Psychiatry 73, 310–312. [PubMed: 12185166]

Sun CX, Robb VA, and Gutmann DH (2002). Protein 4.1 tumor suppressors: getting a FERM grip on growth regulation. J Cell Sci 115, 3991–4000. [PubMed: 12356905]

Taylor AM, Saifetiarova J, and Bhat MA (2017). Postnatal Loss of Neuronal and Glial Neurofascins Differentially Affects Node of Ranvier Maintenance and Myelinated Axon Function. Front Cell Neurosci 11, 11. [PubMed: 28217083]

Trapp BD, Peterson J, Ransohoff RM, Rudick R, Mork S, and Bo L (1998). Axonal transection in the lesions of multiple sclerosis. N Engl J Med 338, 278–285. [PubMed: 9445407]

Tsai J, Grutzendler J, Duff K, and Gan WB (2004). Fibrillar amyloid deposition leads to local synaptic abnormalities and breakage of neuronal branches. Nat Neurosci 7, 1181–1183. [PubMed: 15475950]

van Wijk E, van der Zwaag B, Peters T, Zimmermann U, Te Brinke H, Kersten FF, Marker T, Aller E, Hoefsloot LH, Cremers CW, et al. (2006). The DFNB31 gene product whirlin connects to the Usher protein network in the cochlea and retina by direct association with USH2A and VLGR1. Human molecular genetics 15, 751–765. [PubMed: 16434480]

Wang L, Zou J, Shen Z, Song E, and Yang J (2012). Whirlin interacts with espin and modulates its actin-regulatory function: an insight into the mechanism of Usher syndrome type II. Human molecular genetics 21, 692–710. [PubMed: 22048959]

Yang J, Liu X, Zhao Y, Adamian M, Pawlyk B, Sun X, McMillan DR, Liberman MC, and Li T (2010). Ablation of whirlin long isoform disrupts the USH2 protein complex and causes vision and hearing loss. PLoS Genet 6, e1000955. [PubMed: 20502675]

SIGNIFICANCE STATEMENT

Axonal cytoskeleton provides the structural bases for proper functioning and organization of myelinated axons. Cerebellum is highly enriched with myelinated fibers and plays a crucial role in locomotor activity and acquisition of the fine motor skills. In this study, we show that two cytoskeletal scaffolding proteins, Band 4.1B and Whirlin, play cooperative role in maintaining proper myelinated axon structure and cerebellar function.

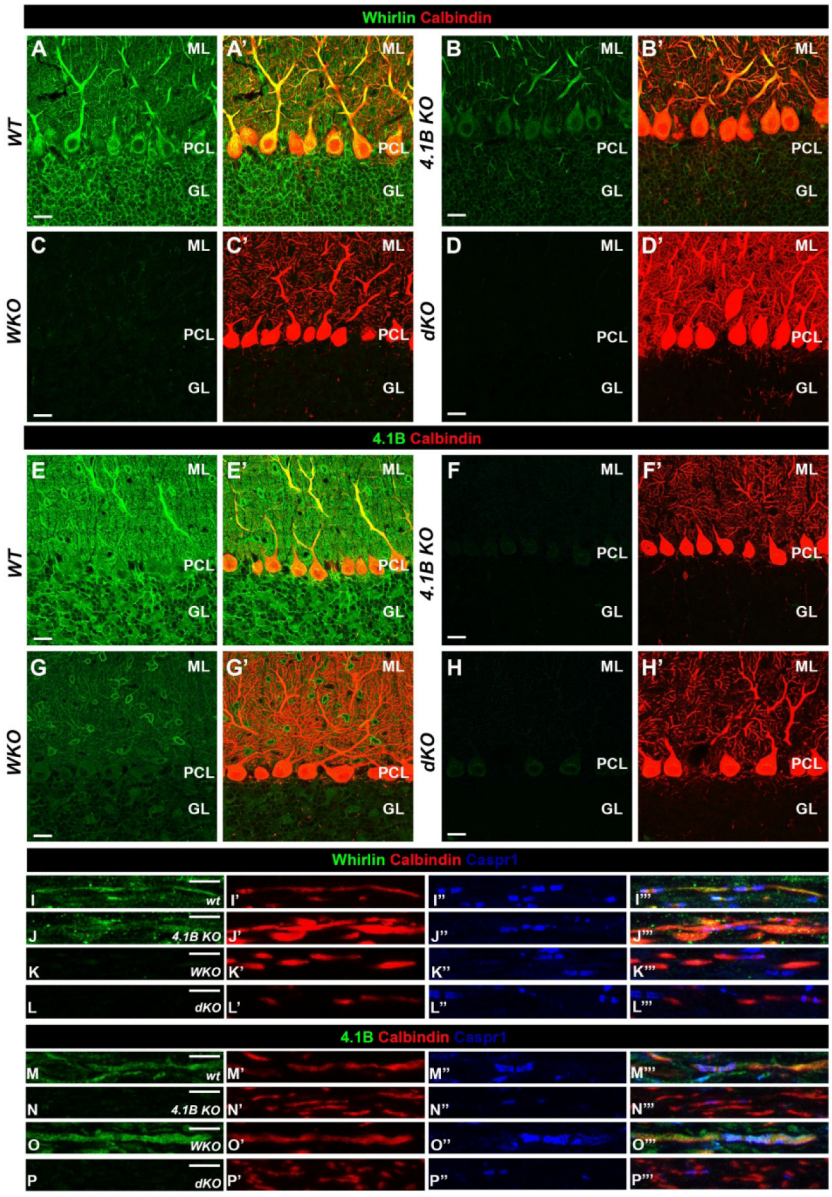

Figure 1. Expression and Subcellular Localization of 4.1B and Whrn in the Cerebellum

A-D) Immunostaining of cerebellar sagittal slices with antibodies against Whrn (green) and calbindin (red) from 2-month old *wt* (A-A'), *4.1B KO* (B-B'), *WKO* (C-C') and *dKO* (D-D') mice. ML, PCL and GCL are molecular layer, Purkinje cell layer and granule cell layer respectively. Scale bar, 20 μm

(E-H) Cerebellar slices from 2-month old *wt* (E-E'), *4.1B KO* (F-P), *WKO* (G-G') and *dKO* (H-H') animals immunolabeled with antibodies against 4.1B (green) and calbindin (red). Scale bar, 20 μm

(I-L) White matter tracts of 2-month old cerebellums from *wt* (I-I'''), *4.1B KO* (J-J'''), *WKO* (K-K''') and *dKO* (L-L''') animals immunostained with antibodies against Whrn (green), calbindin (red) and Caspr1 (blue). Scale bar, 5 μm

(M-P) Cerebellar white matter tracts of 2-month old *wt* (M-M'"), *4.1B KO* (N-N'"), *WKO* (O-O'") and *dKO* (P-P'") mice immunostained with antibodies against 4.1B (green), calbindin (red) and Caspr1 (blue). Scale bar, 5 μm

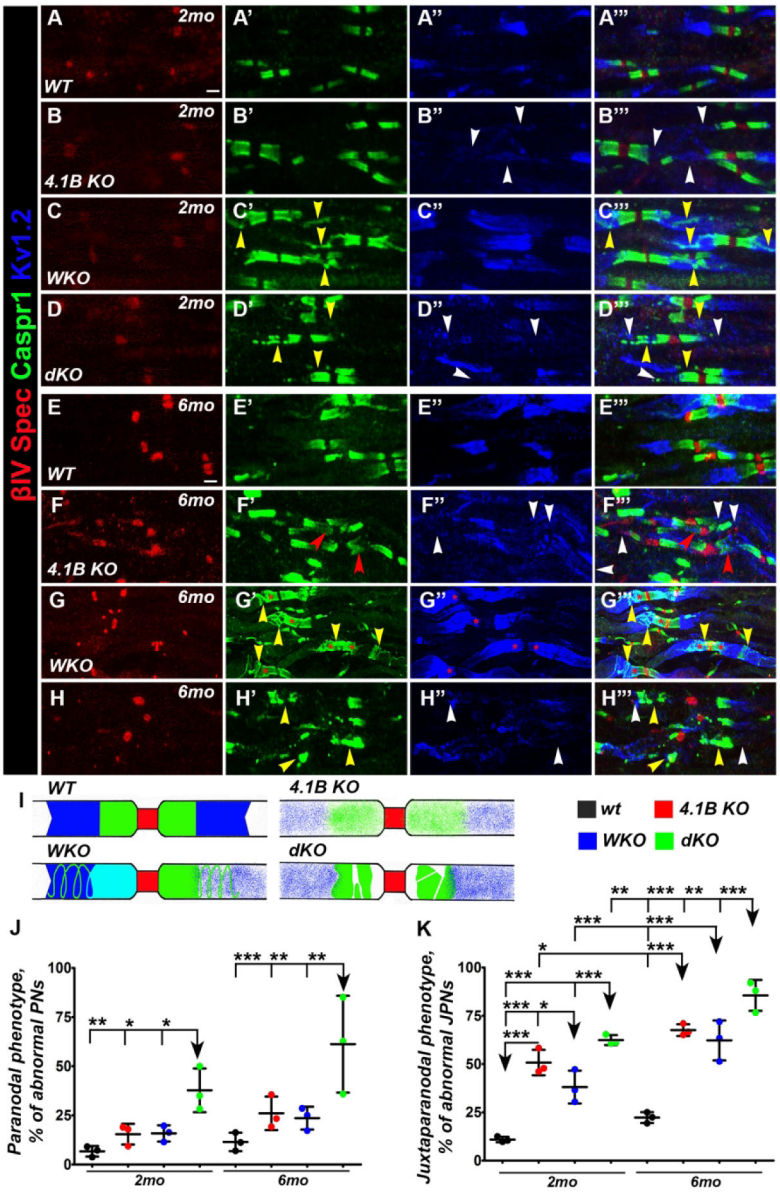

Figure 2. 4.1B and Whrn Maintain Molecular Domain Integrity in Purkinje Neuron Myelinated Axons

(A-H) CB slices from 2-month old *wt* (A-A'"), *4.1B KO* (B-B'"), *WKO* (C-C'") and *dKO* (D-D'"), as well as from 6-month old *wt* (E-E'"), *4.1B KO* (F-F"), *WKO* (G-G'") and *dKO* (H-H'") mice immunostained with antibodies against βIV Spec (red), Caspr1 (green) and $K_{V1.2}$ (blue). Note, that at 2 months in the cerebellar white matter *4.1B KO* animals show normal paranodal organization, however, juxtaparanodal $K_{V1.2}$ localization is disrupted (B''-B''', white arrowheads). *WKO* mice exhibits paranodal pathology, which is manifested by despiralization phenotype (C', C''', yellow arrowheads). *dKO* mice acquire enhanced phenotype, which combines loss/despiralization of paranodes together with mislocalization of juxtaparanodal $K_{V1.2}$ (D'-D''', yellow and white arrowheads, respectively). In 6-month old *4.1B KO* animals paranodes become affected (F', F''', red arrowheads) and

juxtaparanodal $K_{V1.2}$ mislocalization phenotype progresses (F''- F''', white arrowheads). Age matched *WKO* animals display severed paranodal despiralization phenotype (G', G''', yellow arrowheads) and moving of juxtaparanodal $K_{V1.2}$ into the paranodal area (G'-G''', red stars). Paranodal (H', H''', yellow arrowheads) and juxtaparanodal (H'', H''', white arrowheads) domains are severely disrupted in 6-month old *dKO* mice. Scale bar, 2 μm

(I) Schematic representation of paranodal and juxtaparanodal phenotypes observed in *wt, 4.1B KO, WKO* and *dKO* mice. In *wt* animals, nodes (red) are flanked by intact paranodes (green) and juxtaparanodes (blue). In *4.1B KO* mice, nodes are surrounded by diffuse para- and juxtaparanodes. *WKO* animals have uncompacted paranodes with spiral-like stretches towards the juxtaparanodal area; juxtaparanodes are either diffuse (blue, right side) or have moved towards the nodal area and overlap with the paranodes (cyan, left side). *dKO* mice show disrupted paranodal and diffuse juxtaparanodal regions.

(J, K) Quantification of paranodal (J) and juxtaparanodal (K) abnormal phenotypes in 2 and 6-month old wt, *4.1B KO, WKO* and *dKO* animals (n=3 mice with at least 300 quantified paranodes (PN) and juxtaparanodes (JPN)/animal. The line bars represent statistical significance across genotypes at 2 and 6 months. The arrow is pointing at the genotype whose phenotype is being compared with other genotypes. All data are represented as scatter plots with mean ± SD. two-way ANOVA with Bonferroni's post-hoc analysis, *P<0.05; **P<0.01; ***P<0.001).

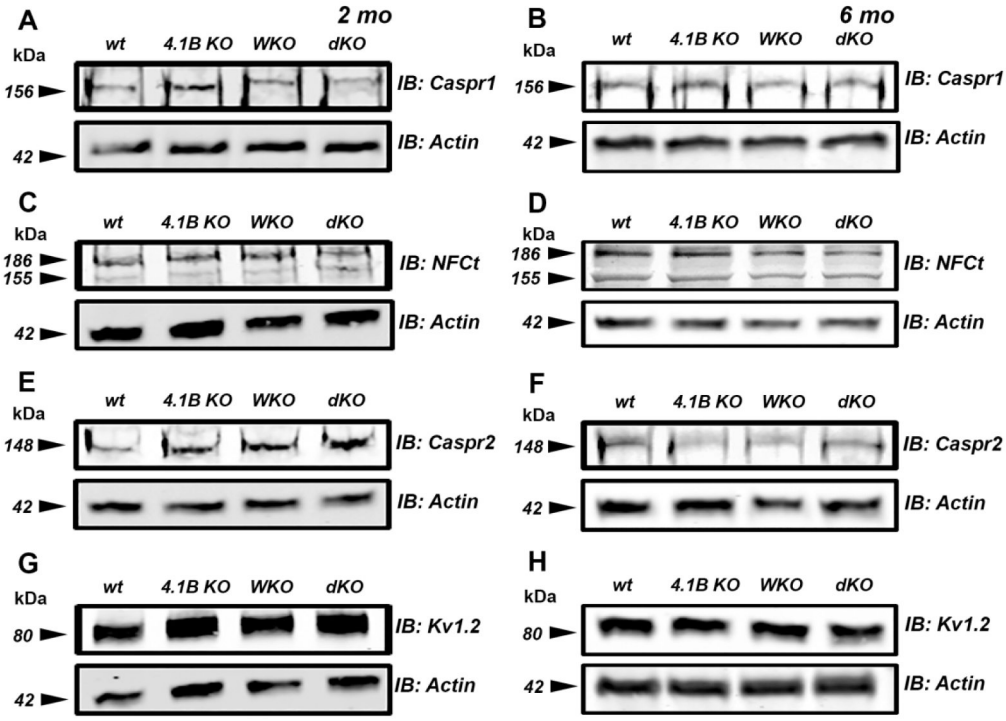

Figure 3. No Effect on Major Paranodal and Juxtaparanodal Proteins Levels After 4.1B and Whrn Ablation

(A-H) Immunoblot analysis of cerebellar lysates from 2- and 6-month old *wt, 4.1B KO, WKO* and *dKO* mice probed with antibodies against Caspr1 (A, B), NFCt (C, D), Caspr2 (E, F) and Kv1.2 (G, H). β-Actin was used for loading control.

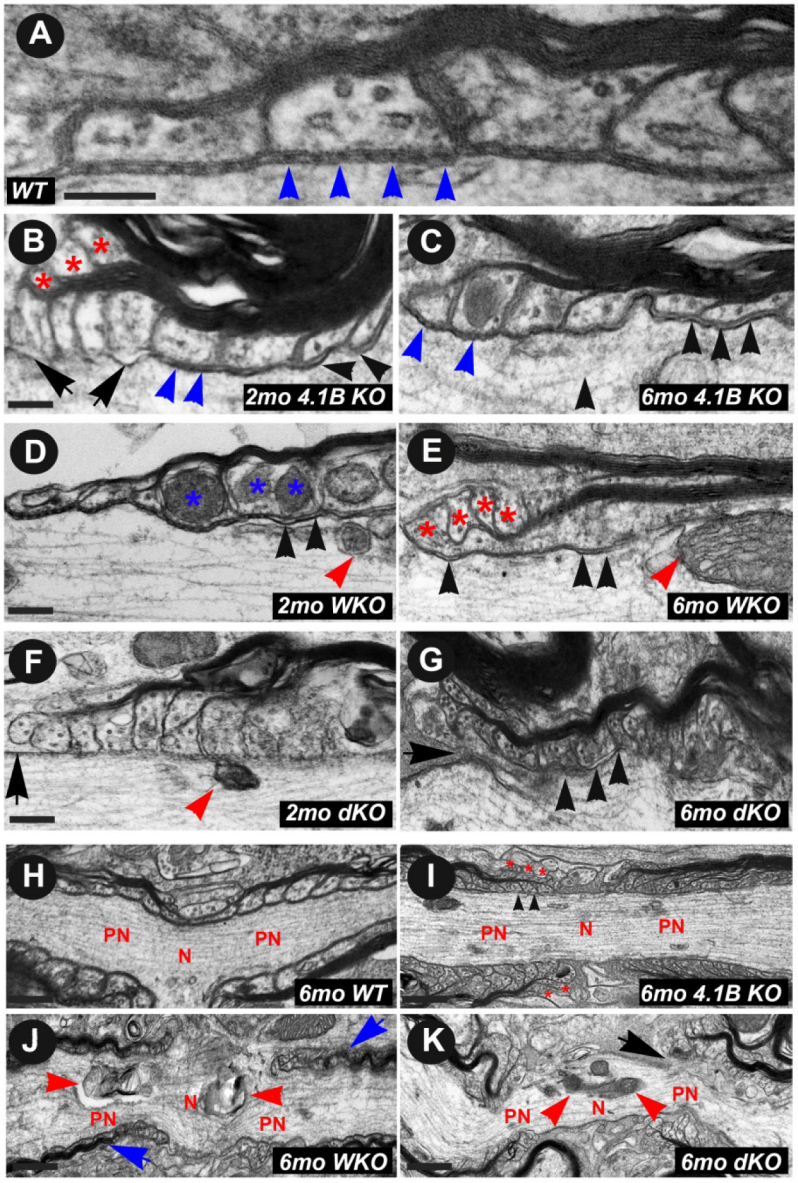

Figure 4. Loss of 4.1B and Whrn Leads to Ultrastructural Disorganization of Myelinated Axons

(A-K) Transmission electron microscopy (TEM) of the cerebellar white matter myelinated axons from 2 and 6 mo *wt* (A, H), *4.1B KO* (B, C, I), *WKO* (D, E, J) and *dKO* (F, G, K) mice. Blue and black arrowheads represent intact and disrupted axo-glial septate junctions, respectively. Red asterisks indicate everted paranodal loops and blue asterisks mark inclusions at the paranodal loops. Black arrows point out at the regions of paranodal detachment from the axolemma. Moreover, blue arrows point at the wavy myelin morphology. Red arrowheads indicate membranous accumulations. Scale bar 100 nm for A; 200 nm for B-G; 500 nm for H-K.

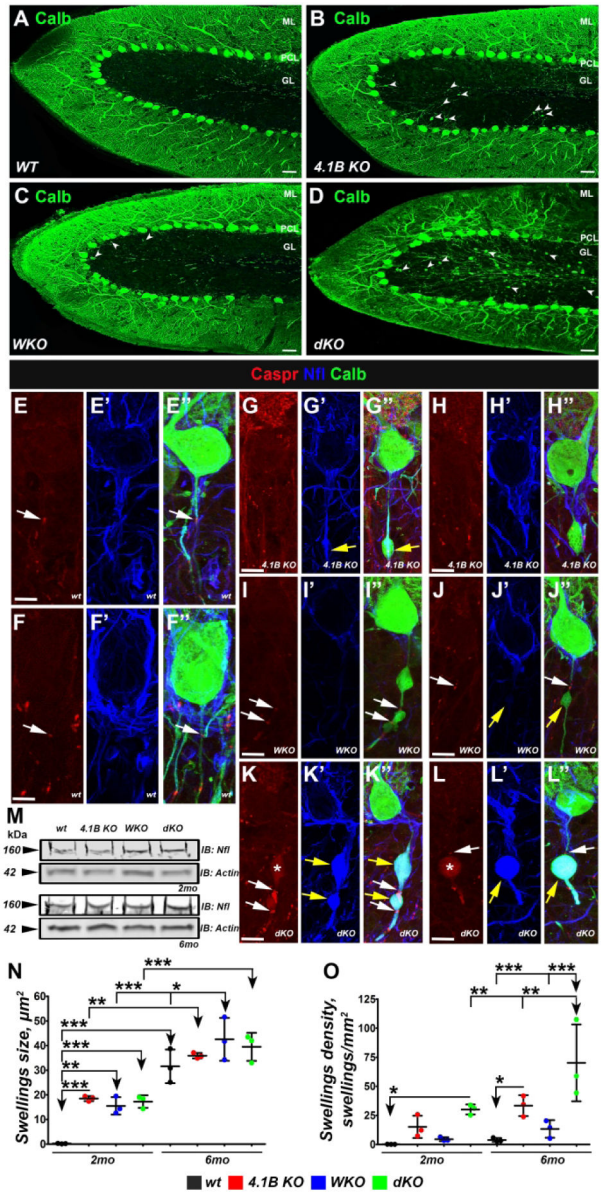

Figure 5. Loss of 4.1B and Whrn Leads to Formation of Axonal Swellings and Purkinje Axon Pathology

(A-D) Immunostaining of cerebellum slices from 6-month old *wt* (A), *4.1B KO* (B), *WKO* (C) and *dKO* (D) with antibodies against Calbindin. Arrows point to swellings along the Purkinje cell fibers. ML, PCL and GCL are molecular layer, Purkinje cell layer and granule cell layer respectively. Scale bar, 50 μm

(E-L) Immunostaining of cerebellum slices from 6-month old *wt* (E-E", F-F"), *4.1B KO* (G-G", H-H"), *WKO* (I-I", J-J") and *dKO* (K-K", L-L") with antibodies against Caspr1 (red), Calbindin (green) and pan-Neurofilament (blue). White arrows indicate Caspr1 positive paranodes along the Purkinje axon. Yellow arrows and white asterisks point at Neurofilament and Caspr1 accumulations within the swellings. Scale bar, 5 μm (M) Immunoblot analysis of cerebellar lysates from 2- and 6-month old *wt, 4.1B KO, WKO* and

dKO mice probed with antibodies against Neurofilament (L) and β-Actin was used for loading control.

(N, 0) Quantifications of the size (N) and density (O) of the swellings in 2– and 6-month old *wt, 4.1B KO, WKO* and *dKO* mice (n=3 mice/genotype per each time point; all data are represented as scatter plots with mean ± SD. The line bars represent statistical significance across genotypes at 2 and 6 months. The arrow is pointing at the genotype whose phenotype is being compared with other genotypes, two-way ANOVA with Bonferroni's post-hoc analysis, *P<0.05; **P<0.01; ***P<0.001).

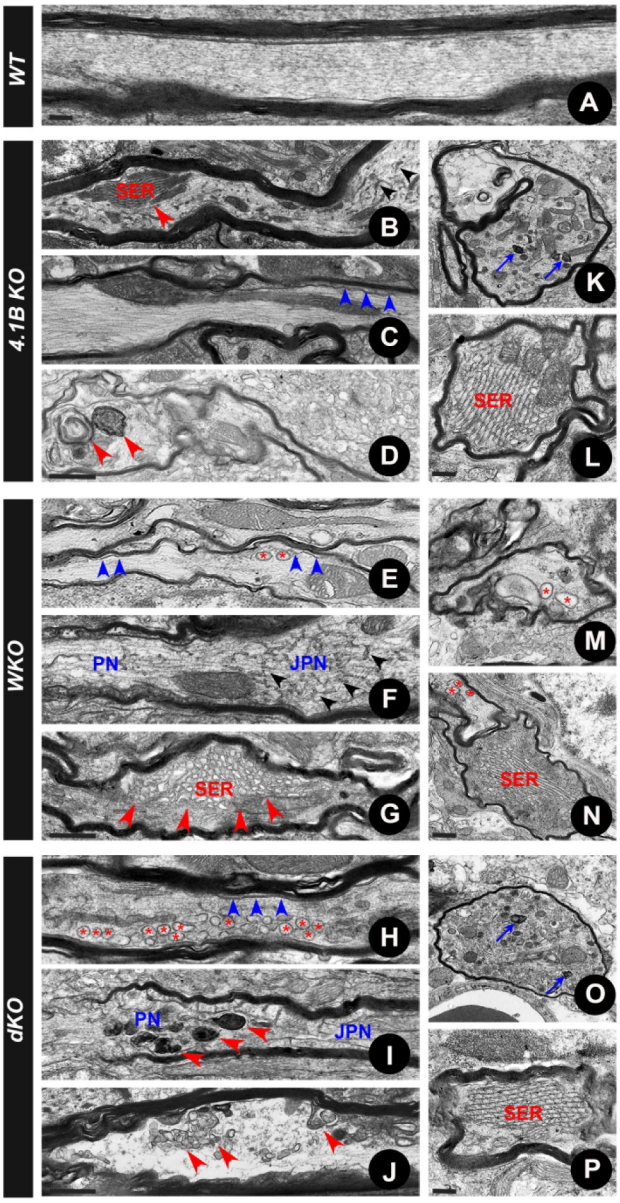

Figure 6. Loss of 4.1B and Whrn Leads to Axonal Cytoskeletal Disruption with Accumulation of Vesicles and Membranous Organelles.

(A-P) TEM of the cerebellar white matter myelinated axons from 6-month old *wt* (A), *4.1B KO* (B-L), *WKO* (E-N) and *dKO* (H-P) mice. Accumulations of membranous organelles is represented by red arrowheads and blue arrows. Detachment myelin sheath from axolemma is marked with blue arrowheads. Accumulations of vesicles is labeled with red asterisks. Scale bar, 600 nm for A-J; 200 nm for K-P.

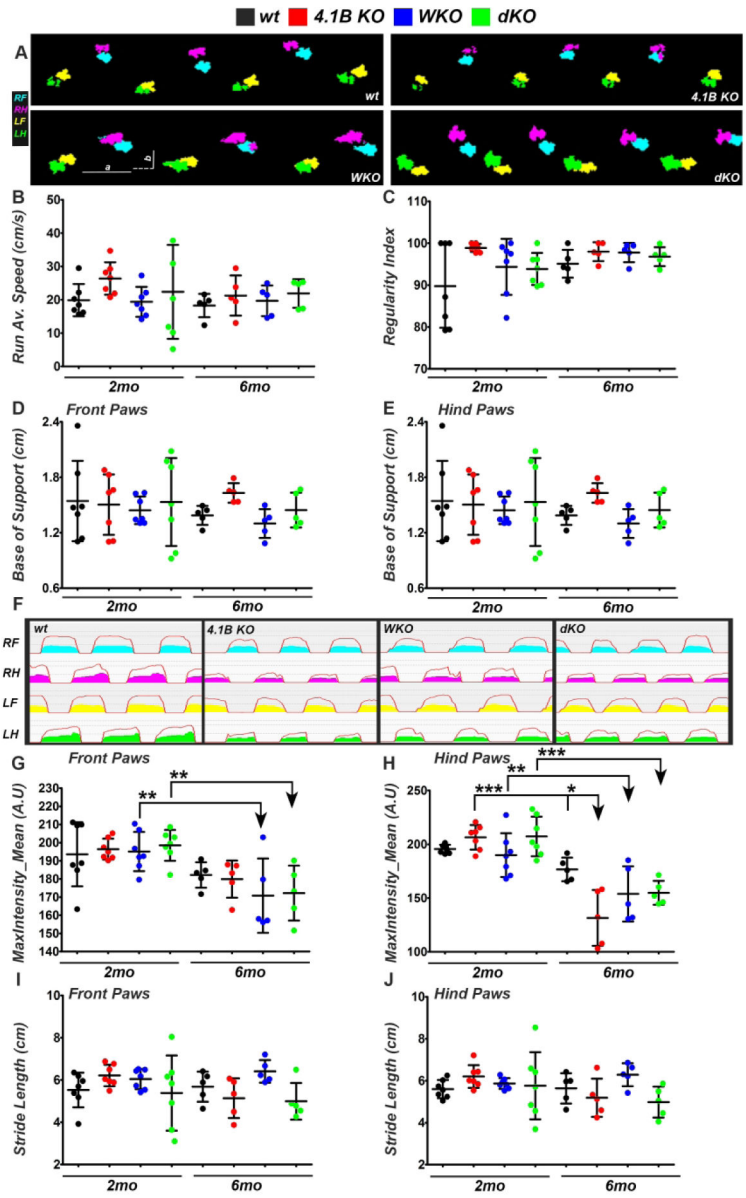

Figure 7. Loss of 4.1B and Whrn Leads to Motor Dysfunction

(A) Representative Catwalk footprints of 6-month old *wt, 4.1B KO, WKO and dKO* mice. (a) line represents the stride length; (b) line represents base of support length.

(B-E) Quantifications of the run average speed (B), regularity index (C) and base of support of the front (D) and hind (E) paws from the catwalk gait recordings of 2- and 6- month old *wt, 4.1B KO, WKO* and *dKO* mice (n= 5-7 mice/genotype).

(F) Representative 2D footprint intensities of the limbs recorded during catwalk gait analysis from *wt, 4.1B KO, WKO and dKO* mice. Solid red line represents the maximum intensity in a frame; the colored area under the red line represents the mean intensity of the paw. *4.1B KO* and *dKO* animals show relatively lower intensity for hind paws, indicating less use of affected paw.

(G-J) Quantifications of the front (G) and hind (H) paws maximal intensities, as well as front (I) and hind (J) paws stride length from the catwalk gait recordings of 2- and 6- month old *wt, 4.1B KO, WKO* and *dKO* mice (n= 5-7 mice/genotype). The line bars represent statistical significance across genotypes at 2 and 6 months. The arrow is pointing at the genotype whose phenotype is being compared with other genotypes (All data are represented as scatter plots with mean ± SD; two-way ANOVA with Bonferroni's post-hoc analysis, *P<0.05; **P<0.01; ***P<0.001).

Table 1.

List of Antibodies Used in This Studies

Antibody	Immunogen	Manufacturer	Concentration
anti-4.1B	amino acids 655–793	Bhat Lab Rabbit polyclonal	1:5000 (IHC)
anti-potassium voltagegated channel subfamily A member 2 (Kv1.2)	amino acids QYLQ-LTDV, cytoplasmic domain	UC Davis/NIH NeuroMab Facility Cat# 75-008 RRID:AB_2296313 mouse monoclonal	1:200 (IHC) 1:1000 (WB)
anti-Neurofilament	phosphorylated axonal epitopes on NF-M and NF-H	Covance Research Products Inc Cat# SMI-312R RRID:AB_2315329 mouse monoclonal	1:200 (IHC)
anti-Whrn	amino acids 220–326, 699-804	Bhat Lab Rabbit polyclonal	1:200 (IHC), 1:2000 (WB),
anti-Caspr1	cytoplasmic domain	Bhat Lab Rabbit polyclonal	1:500 (IHC), 1:2000 (WB),
anti-Calbindin	bovine kidney calbindin-D	Sigma-Aldrich Cat# C9848, RRID:AB_476894 mouse monoclonal	1:200 (IHC)
anti-Calbindin	Calbindin D-28K human, mouse, rat	Millipore Cat#AB1778, RRID:AB_2068336 Rabbit polyclonal	1:200 (IHC)
anti-NFCt	amino acids FIKR-YSLA, cytoplasmic domain	Bhat Lab Rat polyclonal	1:2000 (WB)
anti-Caspr2	CNTNAP2 human, mouse	Abeam Cat# ab33994, RRID:AB_2083506 Rabbit polyclonal	1:2000 (WB)
anti-β-Actin	β-Actin human, bovine, sheep, pig, rabbit, cat, dog, mouse, rat, guinea pig, chicken, carp, leech	Sigma-Aldrich Cat# A5441, RRID:AB_476744 mouse monoclonal	1:5000 (WB)
anti-βIV Spectrin	amino acids ARRA-QESA	Bhat Lab guinea pig, Rabbit polyclonal	1:500 (IHC)

IHC-Immunohistochemistry
WB – Western Blot